Journal of Inorganic Biochemistry 158 (2016) 45–54

Contents lists available at ScienceDirect

Journal of Inorganic Biochemistry

journal homepage: www.elsevier.com/locate/jinorgbio

# Strained ruthenium metal–organic dyads as photocisplatin agents with dual action

Tariq Sainuddin, Mitch Pinto, Huimin Yin, Marc Hetu, Julie Colpitts, Sherri A. McFarland *

*Department of Chemistry, Acadia University, Wolfville, Nova Scotia B4P 2R6, Canada*

ARTICLE INFO

*Article history:*
Received 16 September 2015
Received in revised form 28 December 2015
Accepted 7 January 2016
Available online 9 January 2016

*Keywords:*
Metal complexes
Photocisplatin agents
DNA photocleavage
Photodynamic therapy
Photochemotherapy
Singlet oxygen sensitization

ABSTRACT

Three strained Ru(II) metal–organic dyads were prepared and characterized by NMR, mass spectrometry, and analytical HPLC to probe whether these constructs could act as multifunctional photochemotherapy (PCT) agents. The compounds incorporated the crowded 6,6′-dimethyl-2,2′-bipyridine (6,6′-dmb) ligand to impart stoichiometric photocisplatin activity, and imidazo[4,5-*f*] [1,10]phenanthroline (IP) appended with *n* thiophene units (*n*T; *n* = 1–3) to add capacity for singlet oxygen sensitization. With visible light activation, each complex of the series underwent rapid and selective photoejection of 6,6′-dmb in less than 10 min, with half-lives ($t_{1/2}$) as short as 46.3 s for $[Ru(6,6'\text{-dmb})_2(IP\text{–}1T)]^{2+}$. Photo-triggered ligand loss slowed with increasing *n*, and was slowest for $[Ru(6,6'\text{-dmb})_2(IP\text{–}3T)]^{2+}$ ($t_{1/2}$ = 273 s). This trend also held for photoadduct formation with DNA; $[Ru(6,6'\text{-dmb})_2(IP\text{–}1T)]^{2+}$ produced relaxed circular DNA at the lowest concentrations. Singlet oxygen yields ($\Phi_\Delta$) increased with *n*, whereby $\Phi_\Delta$ for $[Ru(6,6'\text{-dmb})_2(IP\text{–}1T)]^{2+}$ was only 3%, but increased to 42% on going to $[Ru(6,6'\text{-dmb})_2(IP\text{–}3T)]^{2+}$. This photosensitization process was reflected by single-strand breaks in the gel-mobility shift assays of $[Ru(6,6'\text{-dmb})_2(IP\text{–}3T)]^{2+}$, but was not discernible for the other compounds. Despite different photochemical and photophysical reactivities, all of the compounds were potent phototoxic agents toward cancer cells ($EC_{50}$ = 1–2 μM) with relatively short compound-to-light intervals and moderate visible light doses. $[Ru(6,6'\text{-dmb})_2(IP\text{–}3T)]^{2+}$ was exceptionally photoactive toward cancer cells at longer intervals ($EC_{50}$ = 200 nM, PI = 750). Phototherapeutic margins increased with *n* due to decreased dark cytotoxicity for the more π-expansive complexes, making metal–organic dyad $[Ru(6,6'\text{-dmb})_2(IP\text{–}3T)]^{2+}$ the best multifunctional PCT agent.



## 1. Introduction

### 1.1. Evolution of photocisplatin agents

The lack of selectivity and drug resistance associated with most anticancer agents has fueled an ongoing interest in prodrugs that selectively destroy malignant tissue. This selectivity may be achieved by targeting some inherent feature that only cancer cells possess, or by applying an external trigger that can exert spatiotemporal control over the activity of the prodrug. Photodynamic therapy (PDT) is an example of the latter, whereby organic sensitizers photogenerate singlet oxygen ($^1O_2$), and other reactive oxygen species (ROS), upon exposure to visible light. This process destroys illuminated cells that have accumulated the photosensitizer (PS). The salient drawback of PDT, however, is its oxygen dependence alongside the poor chemical characteristics of the few approved organic PSs for PDT.

It is widely known in the field of cancer research that the most aggressive and drug-resistant tumors are hypoxic [1,2]. Recent efforts in the more broadly defined field of photochemotherapy (PCT) are thus aimed at identifying systems that do not require oxygen to elicit a phototoxic effect. Metallodrug PSs are especially attractive in this respect as they possess a variety of triplet excited state configurations that can be accessed through rational design: metal-to-ligand charge transfer (MLCT), metal-centered (MC) or ligand field (LF), ligand-centered (LC) or intraligand (IL), intraligand charge transfer (ILCT), metal-to-metal charge transfer (MMCT), and combinations thereof. Such states can conceivably participate in sensitization processes, redox reactions, covalent modifications, and other pathways with the potential to compromise cell function.

More than two decades ago it was recognized that thermally inert octahedral metal complexes could be activated with light to mimic the thermal chemistry between cisplatin and DNA [3]. Such activity is oxygen-independent and characterized by the photochemical release of labile ligands from dissociative $^3$MC excited states (Scheme 1). Depending on the proximity of the ligand deficient metal to biological targets, the vacant sites can temporarily coordinate solvent or react directly with Lewis bases such as DNA nucleobases. Disruption of the topological integrity of DNA is the key mechanism by which cisplatin exerts both its desirable and undesirable cytotoxic effects. The opportunity to control this process with light using photoactive metal complexes presents an opportunity to eliminate the debilitating side effects associated with cisplatin. Likely in recognition of the pivotal

* Corresponding author.
*E-mail address:* sherri.mcfarland@acadiau.ca (S.A. McFarland).

http://dx.doi.org/10.1016/j.jinorgbio.2016.01.009
0162-0134/

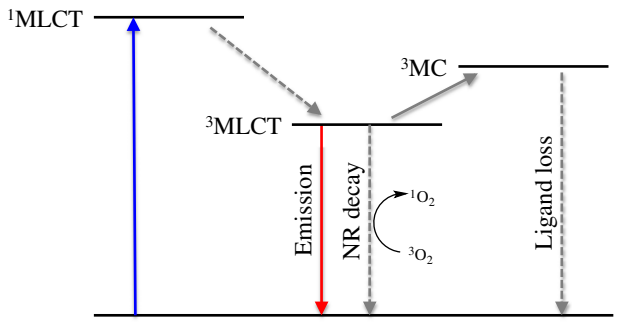


**Scheme 1.** Simplified Jablonski diagram showing excited state decay processes in Ru(II) coordination complexes.

role that cisplatin has played in anticancer therapy and the desire to mimic its favorable properties, such compounds (regardless of the metal employed) have been called *photocisplatin* agents [3,4].

The use of steric bulk to populate $^3$MC excited states that promote ligand dissociation has been demonstrated for complexes of the type $[Ru(biq)(phen)_2]^{2+}$ and $[Ru(phen)_2(biq)]^{2+}$, where phen = [1,10]phenanthroline and biq = 2,2′-biquinoline [5]. The energies of $^3$MC states can also be lowered below $^3$MLCT levels by appending chelating 2,2′-bipyridine (bpy) ligands with simple methyl- or phenyl-groups that point toward the coordination sphere of the metal ion [6–8]. The resulting geometric distortions produce systems that can be activated with visible light to act as photocisplatin agents toward cancer cells with high potency and low dark toxicity (Scheme 2). Turro and coworkers have shown that the introduction of steric clash in $[Ru(tpy)(LL)(L)]^{2+}$ (tpy = 2,2′:2′,6′′-terpyridine; L = monodentate ligand; LL = crowded bidentate ligand) complexes also effects ligand dissociation with light exposure [9], and have recently extended these one-dimensional systems to create multifunctional agents that undergo more than one useful process upon light activation [10,11].

### 1.2. Strained metal–organic dyads as multifunctional cisplatin agents

Our group has an interest in developing metal–organic dyads as potent and versatile PSs for PCT, also known as photoactivated cancer therapy (PACT). A key feature of these systems is a π-expansive ligand that is either contiguously fused to or tethered to an organic chromophore that imparts a low-energy $^3$IL state that is highly photosensitizing and extremely sensitive to trace oxygen [12–18]. The metal center facilitates intersystem crossing (ISC) to the triplet manifold, and the organic chromophore serves to reduce ISC rates from the triplet manifold back to the ground state. The result is a PS with ample time to sensitize reactive intermediates and/or react with biological targets. To our knowledge, these constructs represent the most potent (picomolar) PCT agents and yield the largest therapeutic margins (>$10^5$) to date.

Hybrid systems (strained dyads) that partition their excited-state reactivity between quasi-catalytic photosensitization and stoichiometric covalent modification of biomolecules represent a new type of phototherapy agent that is poised to take advantage of the local microenvironment of tumors. Such agents are designed to utilize oxygen and other photodynamic mediators when they are present, but possess the ability to act as non-sensitizing photocisplatin agents when they are absent. Herein, we propose to equip Ru(II) dyads derived from α-oligothiophenes [12] with photocisplatin activity to yield multifunctional PCT agents (Chart 1).

### 1.3. Rationale for target structures

Glazer and coworkers have shown that the methyl groups of 6,6′-dimethyl-2,2′-bipyridyl (6,6′-dmb) add steric bulk to otherwise stable Ru(II) complexes [6]. The resulting strain distorts the geometry of the pseudo octahedral complex, thus making $^3$MC states accessible with $^1$MLCT absorption in complexes of the type $[Ru(bpy)_2(6,6'\text{-dmb})]^{2+}$. While one 6,6′-dmb ligand is sufficient for strain-mediated photoactivation, we chose a bis-heteroleptic framework with two crowded ligands in order to incorporate a π-expansive ligand without the need for additional synthetic steps required to prepare tris-heteroleptic Ru(II) systems.

The imidazo[4,5-*f*] [1,10]phenanthroline (IP) ligand is a convenient scaffold for appending thienyl substituents as organic chromophores for sensitization; thiophene (1T), 2,2′-bithiophene (2T), 2′,2′′:5′′,2′′′-terthiophene (3T) were employed in this study to probe the effects of π-expansion on the dual reactivity predicted for strained metal–organic complexes 1–3. The $^1O_2$ quantum yields ($\Phi_\Delta$) for the corresponding unstrained polypyridyl systems $[Ru(bpy)_2(IP\text{-}nT)]^{2+}$ (bpy = 2,2′-bipyridine; *n* = number of thiophene units) were previously reported [12], and increase with *n*. The most π-expansive IP–3T ligand gave rise to complexes with unity $\Phi_\Delta$ values, followed by 75% for IP–2T and 50% for IP–1T. Therefore, it was hypothesized that although all three strained systems would act as photocisplatin agents, compound **3** would produce the largest $^1O_2$ yields and be most likely to act as a multifunctional PCT agent.

## 2. Experimental procedures

### 2.1. Materials

1,10-Phenanthroline (phen), 6,6′-dimethyl-2,2′-dipyridyl (6,6′-dmb), 2-thiophene carboxaldehyde, 2,2′-bithiophene-5-carboxaldehyde, 2,2′:5′,2′′-terthiophene-5-carboxaldehyde, ammonium acetate, and $RuCl3 \cdot xH_2O$ were purchased from Sigma-Aldrich and used without further purification. Spectroscopic-grade solvents were purchased from Caledon Laboratory Chemicals. Plasmid pUC19 DNA was purchased from New England BioLabs and transformed using NovaBlue Singles Competent Cells purchased from Novagen. Transformed pUC19 was purified using the QIAprep Spin Miniprep Kit purchased from Qiagen (yield ~62 μg of plasmid DNA per 20 mL culture), and its concentration was determined from its absorbance ($A_{260}$) using ε = 12,824 $M^{-1}$ $cm^{-1}$ (base pairs); purity was estimated by relative absorption at 260 and 280 nm ($A_{260}/A_{280}$ ~ 1.8). Characterized fetal bovine serum (FBS)(VWR), RPMI 1640 (Corning Cellgro) was purchased from VWR. Human promyelocytic leukemia cells (HL-60) were procured from the American Type Culture Collection. Prior to use, FBS was divided into 40-mL aliquots that were heat inactivated (30 min, 55 °C) and subsequently stored at −20 °C. Water for biological experiments was deionized to a resistivity of 18 MΩ cm using a Barnstead filtration system.

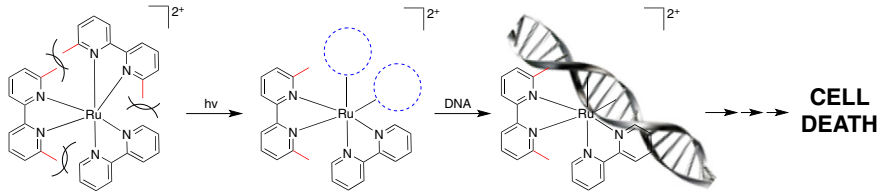


**Scheme 2.** General Mechanism for Photocisplatin Agents.

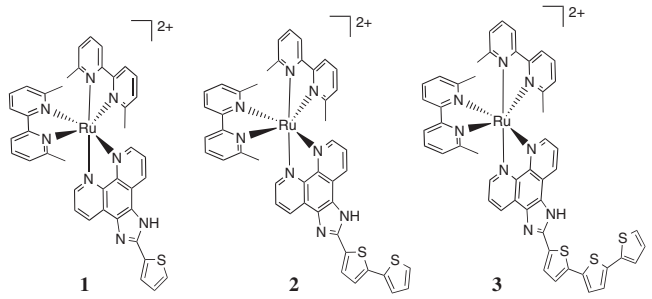

**Chart 1.** Strained Ru(II) metal–organic dyads investigated in this study.

### 2.2. Instrumentation

Microwave reactions were performed in a CEM Discover microwave reactor. NMR spectra were collected using a Bruker AV 500 MHz spectrometer (Dalhousie University Nuclear Magnetic Resonance Research Resource), and ESI mass spectra were obtained using a Bruker microTOF focus mass spectrometer (Dalhousie University Mass Spectrometry Laboratory). HPLC analyses were carried out on an Agilent/Hewlett - Packard 1100 series instrument (ChemStation Rev. A. 10.02 software) using a Hypersil GOLD C18 reversed-phase column with an A–B gradient (98%→40% A; A = 0.1% formic acid in $H_2O$, B = 0.1% formic acid in MeOH). Reported retention times are correct to within ±0.1 min.

### 2.3. Synthesis

The preparation and characterization of compounds **1–3** have not been previously reported. [Ru(6,6′-dmb)2Cl2]·$2H_2O$ was prepared by an established procedure [19], and the three thienyl-appended (n = 1, 1T; n = 2, 2T; n = 3, 3T) imidazo[4,5-*f*][1,10]-phenanthroline (IP) ligands were synthesized using methods previously reported by our group [12]. The metal complexes for this study were isolated and purified as their $PF_6^-$ salts for ease of manipulation, and subsequently subjected to anion metathesis on Amberlite IRA-410 with MeOH to yield the more water-soluble $Cl^-$ salts for photochemical and biological experiments. $^1$H NMR and electrospray ionization ESI (+ve) mass spectra were collected on $PF_6^-$ salts in MeCN-$d_3$ and MeCN, respectively.

[Ru(6,6′-dmb)$_2$(IP–1T)]($PF_6$)$_2$ (**1**). [Ru(6,6′-dmb)$_2$$Cl_2$]·$2H_2O$ (144 mg, 0.25 mmol) and IP–1T (60 mg, 0.20 mmol) were added to a microwave vessel containing ethylene glycol (3 mL). The mixture was subjected to microwave irradiation at 180 °C for 15 min. The resulting dark red solution was loaded directly onto silica gel, eluting first with 100% MeCN, and then with 10% $H_2O$ in MeCN to remove excess starting materials and other impurities. Finally, the desired complex was eluted as a red band with 5% $H_2O$ and 0.5% sat'd $KNO_3$ in MeCN to give a red solid as a mixture of $Cl^-$ and $NO_3^-$ salts. The mixture was converted to the corresponding $PF_6^-$ salt by dissolving in 5–10 mL of water and adding 1–2 mL of sat'd $KPF_6$ to precipitate the desired $PF_6^-$ salt. Subsequent extraction of the aqueous solution with dichloromethane and concentration under reduced pressure gave the pure $PF_6^-$ salt as a dark red solid (209 mg, 98%): $R_f$ = 0.55 (10% $H_2O$ + 2.5% sat'd $KNO_3$ in MeCN). $^1$H NMR (500 MHz, Acetonitrile-$d_3$) δ 8.87 (d, *J* = 8.3 Hz, 2 H; c,f), 8.56 (d, *J* = 8.1 Hz, 2 H; 3′), 8.35 (d, *J* = 8.1 Hz, 2 H; 3), 8.21 (t, *J* = 8.0, 8.0 Hz, 2 H; 4′), 8.18 (dd, *J* = 5.5, 1.2 Hz, 2 H; a,d), 7.94 (d, *J* = 3.7 Hz, 1 H; g), 7.74 (dd, *J* = 8.2, 5.4 Hz, 2 H; b,e), 7.69–7.65 (m, 3 H; 4′,i), 7.58 (dd, *J* = 7.8, 1.2 Hz, 2 H; 5′), 7.28 (dd, *J* = 5.0, 3.7 Hz, 1 H; h), 6.88 (dd, *J* = 7.7, 1.2 Hz, 2 H; 5), 1.91 (s, 6 H; 6′-Me), 1.55 (s, 6 H; 6-Me); MS (ESI+) *m/z* 917.1 [M-$PF_6$]$^+$, 771.1 [M-2$PF_6$-H]$^+$, 386.1 [M-2$PF_6$]$^{2+}$. HRMS ESI+ *m/z* for $C_{41}H_{34}N_8SRu$: cald 386.0355, found 386.0841; HPLC retention time: 9.60 min.

[Ru(6,6′-dmb)$_2$(IP–2T)]($PF_6$)$_2$ (**2**). [Ru(6,6′-dmb)$_2$$Cl_2$]•$2H_2O$ (144 mg, 0.25 mmol) and IP–2T (77 mg, 0.20 mmol) were added to a microwave vessel containing ethylene glycol (3 mL). The mixture was subjected to microwave irradiation at 180 °C for 15 min. The resulting dark red solution was loaded directly onto silica gel, and isolated as described for compound **1** as a mixture of $Cl^-$ and $NO_3^-$ salts. The mixture was diluted in $H_2O$ (5–10 mL), precipitated with 1–2 mL of sat'd $KPF_6$, and vacuum filtered using a fine glass-sintered frit. The solid product was washed with water and diethyl ether to yield the pure $PF_6^-$ salt as a red solid (145 mg, 63%): $R_f$ = 0.62 (10% $H_2O$ + 2.5% sat'd $KNO_3$ in MeCN). $^1$H NMR (500 MHz, Acetonitrile-$d_3$) δ 8.86 (dd, *J* = 8.2, 1.3 Hz, 2 H; c,f), 8.56 (d, *J* = 8.0 Hz, 2 H; 3′), 8.35 (d, *J* = 8.1 Hz, 2 H; 3), 8.21 (t, *J* = 8.0 Hz, 2 H; 4′), 8.18 (dd, *J* = 5.5, 1.2 Hz, 2 H; a,d), 7.85 (d, *J* = 3.9 Hz, 1 H; g), 7.74 (dd, *J* = 8.3, 5.4 Hz, 2 H; b,e), 7.67 (t, *J* = 7.9 Hz, 2 H; 4), 7.58 (dd, *J* = 7.9, 1.4 Hz, 2 H; 5′), 7.48 (dd, *J* = 5.1, 1.1 Hz, 1 H; k), 7.45 (dd, *J* = 3.6, 1.1 Hz, 1 H; i), 7.39 (d, *J* = 3.9 Hz, 1 H; h), 7.16 (dd, *J* = 5.1, 3.6 Hz, 1 H; j), 6.89 (dd, *J* = 7.7, 1.2 Hz, 2 H; 5), 1.91 (s, 6 H; 6′-Me), 1.55 (s, 6 H; 6-Me). MS (ESI+) *m/z* 999.1 [M-$PF_6$]$^+$, 853.1 [M-2$PF_6$-H]$^+$, 427.1 [M-2$PF_6$]$^{2+}$; HRMS ESI+ *m/z* for $C_{45}H_{36}N_8S_2Ru$: cald 427.0774, found 427.0761; HPLC retention time: 20.0 min.

[Ru(6,6′-dmb)$_2$(IP-3T)]($PF_6$)$_2$(**3**). [Ru(6,6′-dmb)$_2$$Cl_2$]•$2H_2O$ (144 mg, 0.25 mmol) and IP–3T (93 mg, 0.20 mmol) were added to a microwave vessel containing ethylene glycol (3 mL). The mixture was subjected to microwave irradiation at 180 °C for 15 min, and isolated according to the procedure described for compound **2** to obtain the pure $PF_6^-$ salt as a red solid (129 mg, 52%): $R_f$ = 0.54 (10% $H_2O$ + 2.5% sat'd $KNO_3$ in MeCN). $^1$H NMR (500 MHz, Acetonitrile-$d_3$) δ 12.16 (s, 1 H; NH), 8.92 (s, 1 H; f), 8.74 (s, 1 H; c), 8.56 (d, *J* = 8.1 Hz, 2 H; 3′), 8.35 (d, *J* = 8.1 Hz, 2 H; 3), 8.24–8.18 (m, 4 H; 4′,a,d), 7.82 (d, *J* = 4.0 Hz, 1 H; g), 7.75 (t, *J* = 7.0 Hz, 2 H; b,e), 7.67 (t, *J* = 7.9 Hz, 2 H; 4), 7.58 (d, *J* = 7.9 Hz, 2 H; 5′), 7.43 (dd, *J* = 5.1, 1.1 Hz, 1 H; h), 7.40 (dd, *J* = 7.7, 3.9 Hz, 2 H; i,j), 7.35 (dd, *J* = 3.6, 1.1 Hz, 1 H; m), 7.28 (d, *J* = 3.8 Hz, 1 H; k), 7.13 (dd, *J* = 5.1, 3.6 Hz, 1 H; l), 6.89 (d, *J* = 7.6 Hz, 2 H; 5), 1.91 (s, 6 H; 6′-Me), 1.56 (s, 6 H; 6-Me). MS (ESI+) *m/z* 1081.1 [M-$PF_6$]$^+$, 935.1 [M-2$PF_6$-H]$^+$, 468.1 [M-2$PF_6$]$^{2+}$; HRMS ESI+ *m/z* for $C_{49}H_{38}N_8S_3Ru$: cald 468.0712, found 468.0701; HPLC retention time: 22.0 min.

### 2.4. Spectroscopy

Absorption spectra were recorded with a Jasco V-530 spectrophotometer, and singlet oxygen emission (centered near 1270 nm) was measured on a PTI Quantamaster equipped with a Hamamatsu R5509-42 near-infrared PMT. Emission and excitation were corrected for the wavelength dependence of lamp output and detector response.

#### 2.4.1. Photoejection

Photoejection experiments were carried out in duplicate in 4.8 × 0.5 × 0.5 cm quartz cuvettes (Starna Cells, Inc.) on 0.8 mL solutions of 20 μM, and visible light irradiation was from a Luzchem LZC-4X photoreactor (7 mW $cm^{-2}$ at the sample) or a 600 W Bell & Howell model 301 transparency projector (125 mW $cm^{-2}$ at the sample). Irradiation intervals were as short as 5 s at early times and more than 300 s at later times; experiments were considered complete when 300-s irradiation intervals produced no further discernible changes in the absorption spectrum. Photoejection kinetics were analyzed by plotting the normalized change in absorption at two wavelengths (on either side of an isosbestic point) against irradiation time using a published method by Glazer and coworkers [5,6,20,21]. The wavelengths selected were those within 50 nm of the longest-wavelength isosbestic point and exhibited the greatest change throughout the course of the experiment. The normalized change in absorption was calculated according to Eq. (1), where *A* represents absorption, and the subscripts 1 and 2 denote wavelength 1 (where absorbance increases with time) and wavelength 2 (where absorbance decreases with time), respectively. The subscript *i* represents the initial absorption at the two wavelengths, and *n* represents the $n^{th}$ data point of absorption at the two wavelengths for

successive irradiation intervals. Plots of $\Delta A$ versus irradiation time were prepared using Graph Pad Prism 6.0 and fit to monoexponential functions to extract rate constants ($k$) and half-lives ($t_{1/2}$) for the photochemical process. Half-life in this context refers to the time it takes to reach ½ of the maximum change in the signal used to monitor the process.

$$\Delta A = (A_{1i} - A_{2i}) - (A_{1n} - A_{2n}) \quad (1)$$

*2.4.2. Singlet oxygen*

Quantum yields for singlet oxygen ($\Phi_\Delta$) production were calculated relative to $[Ru(bpy)_3](PF_6)_2$ ($\Phi_\Delta = 0.56$ in aerated MeCN) [22] according to Eq. (2), where $I$, $A$, and $\eta$ are integrated emission intensity, absorbance at the excitation wavelength, and refractive index of the solvent, respectively. Experiments were performed in triplicate on the $PF_6^-$ salts of compounds **1**–**3** in MeCN (0.8 mL in volume, 5 μM), and emission was collected between 1200 and 1350 nm using a 1000-nm long-pass filter. Excitation was at the longest wavelength excitation maximum for emission at 1270 nm: $\lambda_{ex} = 460$, 465, and 466 nm for **1**–**3**, respectively. Quantum yields were reproducible to within ±10%.

$$\Phi_{em} = \Phi_s \left(\frac{1}{A}\right)\left(\frac{A_s}{I_s}\right)\left(\frac{n^2}{n_s^2}\right) \quad (2)$$

*2.5. Cellular assays*

*2.5.1. Metal compound solutions*

Stock solutions of the chloride salts of the Ru(II) complexes were prepared at 5 mM in 10% DMSO in water and kept at −20 °C prior to use. Working solutions were made by diluting the aqueous stock with pH 7.4 Dulbecco's phosphate buffered saline (DPBS). DPBS is a balanced salt solution of 1.47 mM potassium phosphate monobasic, 8.10 mM sodium phosphate dibasic, 2.68 mM potassium chloride, and 0.137 M sodium chloride (no $Ca^{2+}$ or $Mg^{2+}$). DMSO in the assay wells was under 0.1% at the highest complex concentration.

*2.5.2. Cell culture*

HL-60. HL-60 human promyelocytic leukemia cells (ATCC CCL-240) were cultured at 37 °C under 5% $CO_2$ in RPMI 1640 (Mediatech Media MT-10-040-CV) supplemented with 20% FBS (PAA Laboratories, A15-701) and were passaged 3–4 times per week according to standard aseptic procedures. Cultures were started at 200,000 cells $mL^{-1}$ in 25 $cm^2$ tissue culture flasks and were subcultured when growth reached 800,000 cells $mL^{-1}$ to avoid senescence associated with prolonged high cell density. Complete media was prepared in 200-mL portions as needed by combining RPMI 1640 (160 mL) and FBS (40 mL, prealiquoted and heat inactivated), in a 250-mL Millipore vacuum stericup (0.22 μm) and filtering.

SK-MEL-28. Adherent SK-MEL-28 malignant melanoma cells (ATCC HTB-72) were cultured in Eagle's Minimum Essential Medium (EMEM, Mediatech Media MT-10-009-CV) supplemented with 10% FBS and were incubated at 37 °C under 5% $CO_2$ and passaged 2–3 times per week according to standard aseptic procedures. SK-MEL-28 cells were started at 200,000 cells $mL^{-1}$ in 75 $cm^2$ tissue culture flasks and were subcultured when growth reached 550,000 cells $mL^{-1}$ by removing old culture medium and rinsing the cell layer once with Dulbecco's phosphate buffered saline (DPBS 1X, Mediatech, 21-031-CV), followed by dissociation of cell monolayer with 1X Trypsin–EDTA solution (0.25% (*w*/*v* Trypsin/0.53 mM EDTA, ATCC 30-2101). Complete growth medium was added to the cell suspension to allow appropriate aliquots of cells to be transferred to new cell vessels. Complete growth medium was prepared in 150-mL portions as needed by combing EMEM (135 mL) and FBS (15 mL, prealiquoted and heat inactivated) in a 250-mL Millipore vacuum stericup (0.22 μm) and filtering.

*2.5.3. Cytotoxicity and photocytotoxicity*

Cell viability experiments were performed in triplicate in 96-well ultra-low attachment flat bottom microtiter plates (Corning Costar, Acton, MA), where outer wells along the periphery contained 200 μL DPBS to minimize evaporation from sample wells. Cells growing in log phase (HL-60 cells: ~800,000 cells $mL^{-1}$; SK-MEL-28 cells: ~550,000 cells $mL^{-1}$) with at least 93% viability were transferred in 50-μL aliquots to inner wells containing warm culture medium (25 μL) and placed in a 37 °C, 5% $CO_2$ water-jacketed incubator (Thermo Electron Corp., FormaSeries II, Model 3110, HEPA Class 100) for 3 h to equilibrate (and allow for efficient cell attachment in the case of SK-MEL-28 adherent cells). Metal compounds were serially diluted with DPBS and prewarmed at 37 °C before 25 μL aliquots of the appropriate dilutions were added to cells. Control wells without added metal complex received 25 μL of DPBS. PS-treated microplates were incubated at 37 °C under 5% $CO_2$ for 1 or 16 h (compound-to-light interval) prior to receiving light or sham (dark) treatments. Sham microplates were kept in the dark in an incubator while light-treated microplates were irradiated with visible light (400–700 nm, 34.2 mW $cm^{-2}$) from a 190 W BenQ MS 510 overhead projector for approximately 49 min to yield a total light dose of 100 J $cm^{-2}$. Both untreated and light-treated microplates were incubated for another 48 h before 10-μL aliquots of prewarmed Alamar Blue reagent (Life Technologies DAL 1025) were added to all sample wells and subsequently incubated for another 15–16 h. Cell viability was determined on the basis of the ability of the Alamar Blue redox indicator to be metabolically converted to a fluorescent dye only by live cells. Fluorescence was quantified with a Cytofluor 4000 fluorescence microplate reader with the excitation filter set at 530 ± 25 nm and emission filter set at 620 ± 40 nm. $EC_{50}$ values for cytotoxicity (dark) and photocytotoxicity (light) were calculated from sigmoidal fits of the dose–response curves using Graph Pad Prism 6.0 according to Eq. (3), where where $y_i$ and $y_f$ are the initial and final fluorescence signal intensities. For cells growing in log phase and of the same passage number, $EC_{50}$ values are generally reproducible to within ±25% in the submicromolar regime; ±10% below 10 μM; and ±5% above 10 μM. Phototherapeutic indices (PIs), a measure of the therapeutic window, were calculated from the ratio of dark to light $EC_{50}$ values obtained from the dose–response curves.

$$y = y_i + \frac{y_i - y_f}{1 + 10^{(\log EC_{50} - x)x(\text{Hill slope})}} \quad (3)$$

*2.6. DNA mobility-shift assays*

DNA modification by compounds **1**–**3** was assessed according to a general plasmid DNA gel mobility shift assay [18,23,24] with 30 μL total sample volumes in 0.5 mL microfuge tubes. Transformed pUC19 plasmid (3 μL, >95% form I) was added to 15 μL of 5 mM Tris–HCl buffer supplemented with 50 mM NaCl (pH 7.5). Serial dilutions of the Ru(II) compounds were prepared in $ddH_2O$ and added in 7.5-μL aliquots to the appropriate tubes to yield final Ru(II) concentrations ranging from 1 to 100 μM. Then ddH2O (4.5 μL) was added to bring the final assay volumes to 30 μL. Control samples with no metal complex received 12 μL of water. Sample tubes were kept at 37 °C in the dark or irradiated. Light treatments employed visible light (14 J $cm^{-2}$) delivered from a Luzchem LZC-4X photoreactor over the course of 30 min. A softer light dose relative to that used in the cellular assays was required in order to see the topological changes to DNA before the DNA became too distorted to be imaged with the intercalating dye. After treatment, all samples (dark and light) were quenched by the addition of 6 μL gel loading buffer (0.025% bromophenol blue, 40% glycerol). Samples (11.8 μL) were loaded onto 1% agarose gels cast with 1 × TAE (40 mM Tris–acetate, 1 mM EDTA, pH 8.2) and electrophoresed for 30 min at 80 V $cm^{-1}$ in 1 × TAE prior to staining for 30 min in an aqueous solution of 2 μg/mL ethidium bromide. The bands were visualized using the Gel

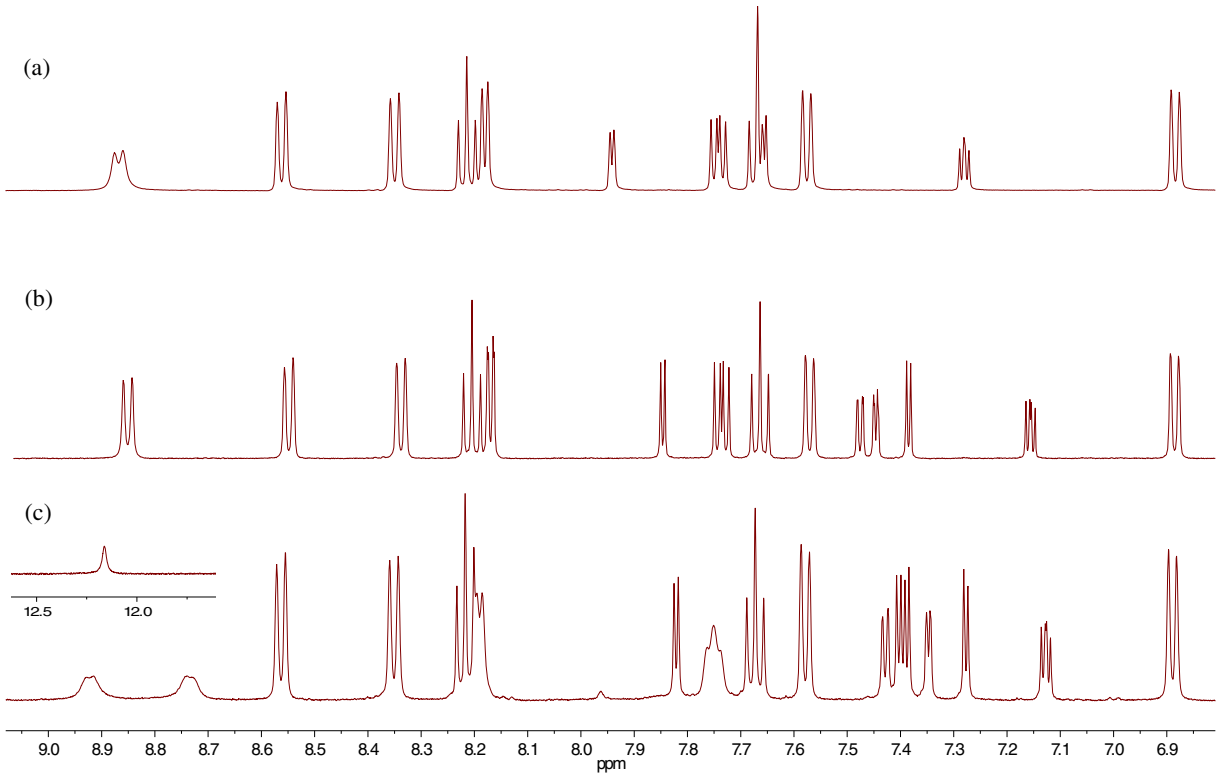


**Fig. 1.** Aromatic regions of the $^1$H NMR spectra collected for compounds **1** (a), **2** (b), and **3** (c) as their $PF_6$ salts in $d_3$-MeCN.

Doc-It Imaging system (UVP) with Vision Works software, and further processed with the GNU Image Manipulation Program (GIMP).

## 3. Results and discussion

### 3.1. Synthesis and characterization

The strained Ru(II) metal–organic dyads were prepared under low-light conditions as racemic mixtures of Δ and Λ enantiomers by reacting $Ru(6,6'\text{-dmb})_2Cl_2$ with the appropriate thienyl-appended IP ligand in ethylene glycol. The crude products were purified on silica gel, and isolated as organic-soluble $PF_6^-$ salts that were characterized by HPLC, 1D and 2D NMR, and mass spectrometry. Each pure complex was also converted to its corresponding water-soluble $Cl^-$ salt for biological testing via anion metathesis on Amberlite IRA-410.

Two dimensional $^1$H–$^1$H COSYNMR was used to definitively assign the signals in the 1D $^1$H spectra collected for complexes **1**–**3** in $d_3$-MeCN (Supporting Information). The diagnostic aliphatic methyl groups 6′-Me and 6-Me were observed as singlets near 1.91 and 1.56 ppm, respectively. The assignments for the polypyridyl hydrogens of the 6,6′-dmb ligands were generally in agreement with those reported for $[Ru(bpy)_2(LL)]^{2+}$ complexes [25–28]. Chemical shifts were in the order of H-3′/3 > H-4′/4 > H-5′/5. The H-3′/3 hydrogens were observed as doublets, H-5′/5 were observed as doublets of doublets, and H-4′/4 appeared as triplets for compound **2**, whereas the H-4′/4 hydrogens for **1** and **3** were observed as overlapping triplets. The signals for the imidazole–NH hydrogens of complexes **1** and **2** were not observed, presumably due to quick exchange (Fig. 1) [29,30]. However, the -NH proton of complex **3** was observed in some spectra at 12.16 ppm, which split H-f and H-c at 8.92 and 8.74 ppm, respectively, into broad singlets. Other NMR spectra collected for complex **3** in MeCN-$d_3$ showed H-c and H-f as one broad doublet at 8.82 ppm with no –NH signal near 12 ppm. The remaining hydrogens of the IP ligands were also assigned by 2D $^1$H-$^1$H COSY NMR spectroscopy.

### 3.2. Photochemistry

All three complexes undergo photochemical ligand dissociation reactions when exposed to visible light, but are substitutionally inert in the dark. Changes in the electronic absorption spectra of **1**–**3** with increasing irradiation time are depicted in Fig. 2. The photochemical reaction followed by UV/Vis absorption was selective for a single process, highlighted by clear isosbestic points near 223, 282, and 482 nm for **1**; 226, 278, and 484 nm for **2**; and 226, 242, and 500 nm for **3**. HPLC analysis of the samples before and after irradiation identified 6,6′-dmb as the photolabile ligand for all of the compounds (Table 1).

Before photolysis, a single peak was observed for each complex with a retention time indicative of increased hydrophobicity of the complex with increasing number of thiophene units. After photolysis with visible light (delivered at 7 mw $cm^{-2}$), two peaks were observed for **1** and **2**: the free 6,6′-dmb ligand at 8.38 min (confirmed by comparison to commercial 6,6′-dmb, which eluted at 8.41 min), and the corresponding Ru(II) aqua complexes (solvated product) at 9.25 and 15.5 min, respectively. Compound **3** did not photoeject completely under these conditions, supported by three peaks in the chromatogram: starting complex at 22 min, alongside the ejected 6,6′-dmb at 8.39 min and the Ru(II) aqua complex at 21.7 min. The production of more polar Ru(II) products with retention times that increase in the order of increasing number of thiophenes also supports the notion that the photochemical reaction is selective for 6,6′-dmb ejection; ejection of the IP–*n*T ligand would have produced identical Ru(II) products and the corresponding free IP–*n*T ligands with different elution times. The proposed photochemical reaction based on analytical HPLC is shown in Scheme 3, whereby the aquated

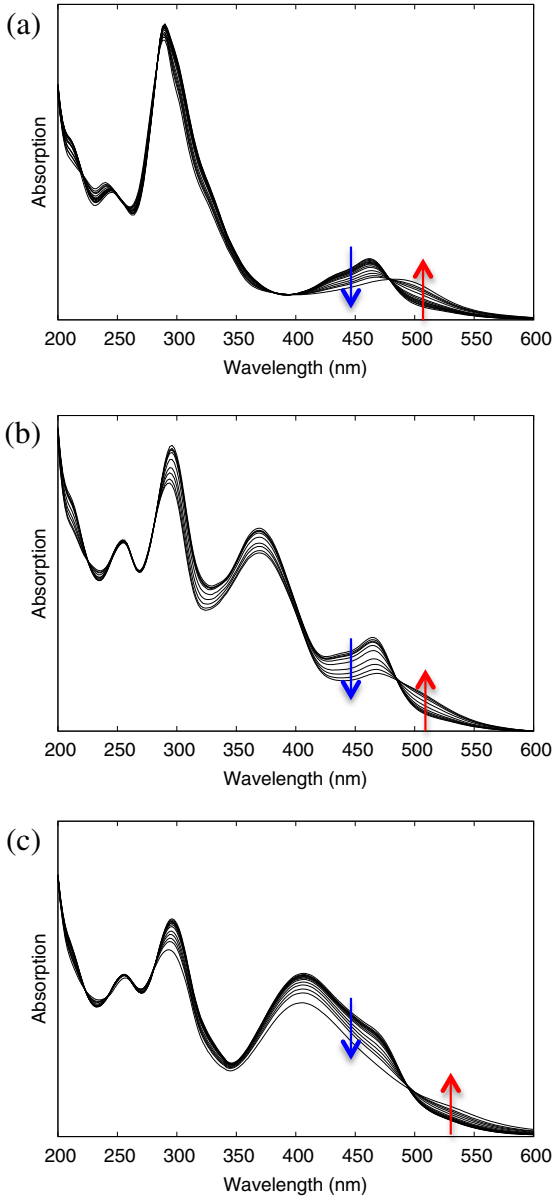


**Fig. 2.** Photoejection of **1**–**3** [(a)–(c), respectively] as $Cl^-$ salts in water monitored by UV/Vis absorption.

Ru(II) intermediate is poised to undergo nucleobase coordination and covalently modify DNA.

The kinetics for photo-triggered ligand dissociation were followed to completion using the conditions that were employed for the analytical HPLC study (Fig. 3).[1] Visible light irradiation from a 7 mW $cm^{-2}$ source produced rapid ligand loss, with $t_{1/2}$ values between 2 and 5 min (Table 2).[2]Despite similar strain inferred for the three complexes produced by identical 6,6′-dmb ligands, the non-labile IP–*n*T ligand had an observable influence on the reaction kinetics. As the number of thiophene units increased from $n = 1$–3, the half-life for photoejection also increased, with the rate being more than two times slower for π-expansive **3** relative to compounds **1** and **2**. This difference was even more pronounced when the light treatment was delivered at a higher energy density (125 mW $cm^{-2}$ vs 7 mW $cm^{-2}$). In this case, **1** photoejected 6,6′-dmb about six times faster than **3** (46.3 vs 273 s), and almost twice as fast as **2** (46.3 vs 84.4 s) Interesting, the increased irradiance had essentially no impact on the photoejection kinetics for compound **3**, pointing toward other pathways that may be equally important for excited state deactivation in π-expansive metal–organic dyads.

**Table 1**
HPLC retention times for non-photolyzed (Dark) and photolyzed (Light) aqueous solutions of strained Ru(II) metal–organic dyads.

| Compd | Retention time (min) | |
|---|---|---|
| | Dark | Light[a] |
| 1 | 9.60 | 9.25, 8.38 |
| 2 | 20.0 | 15.5, 8.38 |
| 3 | 22.0 | 22.0, 21.7, 8.39 |
| 6,6′-dmb | 8.41 | 8.41 |

[a] Photolysis with visible light from a photoreactor (7 mW $cm^{-2}$).

### 3.3. DNA photobinding

DNA damage inflicted by compounds **1**–**3** was probed by agarose gel electrophoresis, as shown in Fig. 4. It is known that cisplatin forms covalent adducts with DNA nucleobases that retard migration of supercoiled plasmid (form I) through the gel (Figure S13) [31]. The unwinding of the DNA helix not only reduces gel electrophoretic mobility, but also can impede intercalation of the ethidium bromide (EtBr) stain used for visualization of DNA bands [32]. Thus, increasing concentrations of cisplatin will cause form I DNA to eventually co-migrate with nicked circular DNA (form II) with gradual disappearance of the bands at high concentrations of the metal complex. This coalescence point defines the concentration of compound required to remove all negative supercoils, producing relaxed plasmid DNA, and is a general measure of the compound's ability to form adducts with DNA.[3]

Photoactivation of compounds **1**–**3** with visible light (14 J $cm^{-2}$ delivered at 7 mW $cm^{-2}$) produced dose-dependent effects on DNA gel electrophoretic mobility in the order **1**>**2**>**3** (Fig. 4). All three compounds compounds, when activated by a light trigger, interacted with DNA more strongly than cisplatin (Figure S13). Lanes 1 and 2 are control lanes that mark the mobility of pUC19 plasmid DNA without the addition of metal complex. Lane 13 is also a control lane showing the effect of the highest concentration of compound (40 μM) on DNA mobility in the dark. Compound **1** had no effect on DNA in the dark, but caused conversion of supercoiled plasmid to its relaxed circular form at compound-to-nucleotide ratios (C/N) as low as 0.38. With increasing number of thiophenes in the IP–*n*T ligand, slightly higher concentrations of compound were required to induce similar topological changes with the same light dose (C/N = 0.75 and 1.25 for **2** and **3**, respectively). By comparison, it took significantly higher concentrations of cisplatin to relax the plasmid (C/N = 3.51), and this DNA damage could not be controlled with light.

At the highest concentrations of compound in the dark, no bands were visible in the presence of **1**–**3**, presumably due to the quenching of EtBr fluorescence by these metal complexes. In these cases, analytical HPLC proved useful in confirming that no photochemical reaction, and thus no adduct formation, had taken place.

Evidence of DNA photocleavage by compound **3** can be seen in lanes 5–8 (Fig. 4) as increased form II band densities, which appears to take place before (or concomitant with) photoadduct formation. This photocleavage by **3** (but not for **1** or **2**) was confirmed by electrophoresis of the DNA products on a gel with EtBr pre-incorporated in the agarose

[1] Intermittent UV/Vis absorption scans (where light is shone on the sample as an inherent part of the experiment) will influence the kinetics by comparison to the analysis by HPLC.

[2] Both the counterion and solvent are expected to influence the photochemical kinetics and mechanism (dissociative vs associative, rechelation, etc.). Note that these values refer to one solvent system and one type of counterion ($Cl^-$ salt in water).

[3] Strong intercalators also unwind DNA and reduce gel mobility, making orthogonal analytical methods crucial in confirming adduct formation.

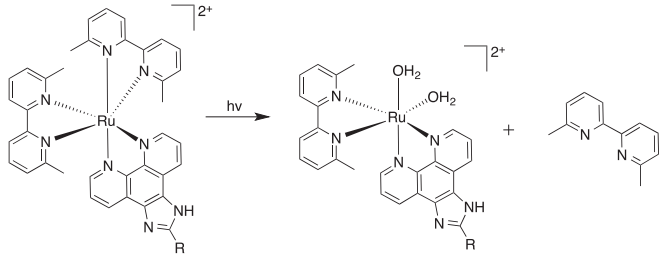


**Scheme 3.** Proposed photolysis reaction based on HPLC analysis.

(0.75 μg $mL^{-1}$ EtBr in 1% agarose), which preferentially highlights DNA damage through the strand breakage mechanism. The ability of **3** to invoke single-strand breaks in DNA in response to a light trigger suggests singlet oxygen ($^1O_2$) sensitization by the metal complex as a parallel pathway. Indeed, the $^1O_2$ quantum yield ($\Phi_\Delta$) for **3** (42%) was over ten-fold larger than that measured for **1** (Table 3). As might be expected, $\Phi_\Delta$ for 2 was between that measured for **1** and **3** at 34%, obeying the same trend outlined for the ligand photoejection kinetics and DNA mobility effects: $\Phi_\Delta$ increases with increasing number of thiophenes, while $t_{1/2}$ values and photoreactivity toward DNA decrease. Nevertheless, it should be noted that these correlations may not be direct. Differences in the relative (non-covalent) DNA binding affinities of the complexes also influence DNA interactions, and were not probed as part of this study. Likewise, pathways other than $^1O_2$ sensitization and photoejection contribute to excited state deactivation, and were not considered.

### 3.4. Cytotoxicity and photocytotoxicity

The biological potencies of the strained metal–organic dyads were assessed in HL-60 human leukemia cells. The HL-60 cell line was chosen

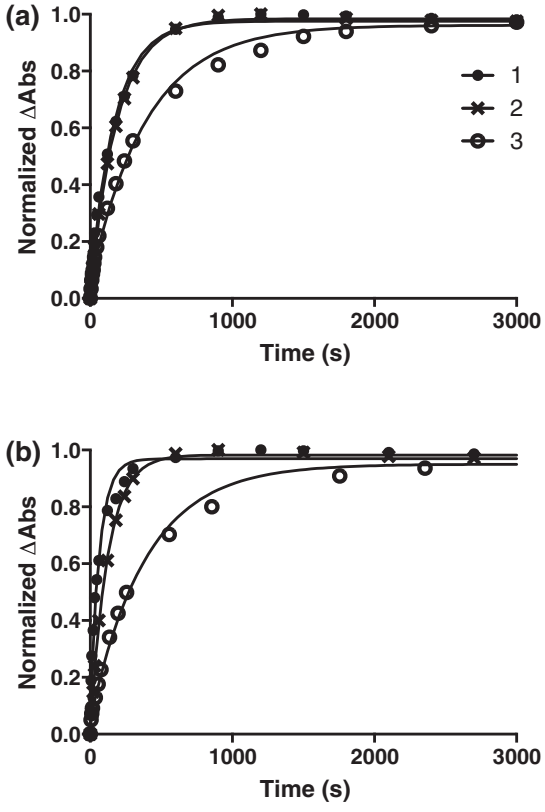


**Fig. 3.** Kinetic fits for the visible-light photolysis of compounds **1**–**3** (followed by changes in UV/Vis absorbance) at two different power densities: (a) 7 mW $cm^{-2}$, and (b) 125 mW $cm^{-2}$.

**Table 2**
Photoejection kinetics measured for compounds **1**–**3** with visible light treatment.

| Compd | Half-life ($t_{1/2}$, s) | |
|---|---|---|
| | 7 mW $cm^{-2}$ | 125 mW $cm^{-2}$ |
| 1 | 122 | 46.3 |
| 2 | 132 | 84.4 |
| 3 | 275 | 273 |

to probe biological activity because it is non-adherent and generally robust. In our experience this cell line is an excellent filter for selecting compounds for further study in more sophisticated models. Briefly, cells were dosed with metal complex (1 nM–300 μM) and allowed to incubate at 37 °C prior to a light (400–700 nm, 100 J $cm^{-2}$) or sham (dark) treatment. Both short (1 h) and long (16 h) compound-to-light intervals ($t_{hν}$) were interrogated in this study. Alamar Blue was added at 48 h post treatment, and cell viability was quantified 16 h later. Cells that were exposed to metal complexes at the highest concentrations (where the compound interferes with the absorption and emission of light by the viability indicator dye) were also counted manually.

With cytotoxicity $EC_{50}$ values exceeding 100 μM (Table 3), compounds **2** and **3** were considered nontoxic to cells under both short and long incubation times in the absence of a light trigger. Compound **1**, on the other hand was cytotoxic, but was significantly less toxic than cisplatin by comparison. At longer incubation times, **1**–**3** became somewhat more cytotoxic, which may be attributed to ongoing cellular accumulation over the additional 15 h period. Regardless of incubation time, dark cytotoxicity in this series decreased with increasing number of thiophene units in the non-labile IP ligand, which may be related to diminished cellular

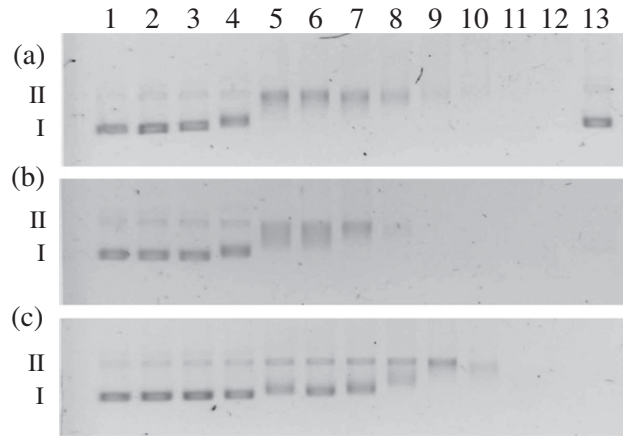


**Fig. 4.** DNA agarose gel mobility shift gels of pUC19 plasmid (20 μM bases) dosed with compound **1** (a), **2** (b), or **3** (c) with (lanes 3–12) or without (lane 13) a light treatment. Lane 1, DNA only ($-hν$); lane 2, DNA only ($+hν$); lane 3, 2.5 μM PS ($+hν$); lane 4, 5 μM PS ($+hν$); lane 5, 7.5 μM PS ($+hν$); lane 6, 10 μM PS ($+hν$); lane 7, 15 μM PS ($+hν$); lane 8, 20 μM PS ($+hν$); lane 9, 25 μM PS ($+hν$); lane 10, 30 μM PS ($+hν$); lane 11, 35 μM PS ($+hν$), lane 12, 40 μM PS ($+hν$); lane 13, 40 μM PS ($-hν$). PS = photosensitizer.

**Table 3**
Photobiological activity in HL-60 cells and singlet oxygen quantum yields measured for compounds **1**–**3**.

| Compd | $EC_{50}$ (μM) | | | | PI | | $\Phi_\Delta$ |
|---|---|---|---|---|---|---|---|
| | Dark | | Light | | | | |
| | 1 h | 16 h | 1 h | 16 h | 1 h | 16 h | |
| 1 | 37 ± 10 | 16 ± 3 | 1.7 ± 0.3 | 1.1 ± 0.7 | 22 | 15 | 0.03 |
| 2 | 154 ± 25 | 115 ± 17 | 1.2 ± 0.2 | 1.2 ± 0.1 | 128 | 96 | 0.34 |
| 3 | 183 ± 17 | 150 ± 8 | 1.1 ± 0.1 | 0.2 ± 0.1 | 166 | 750 | 0.42 |
| Cisplatin | 5.9 ± 0.3 | 2.8 ± 0.1 | - | - | - | - | - |

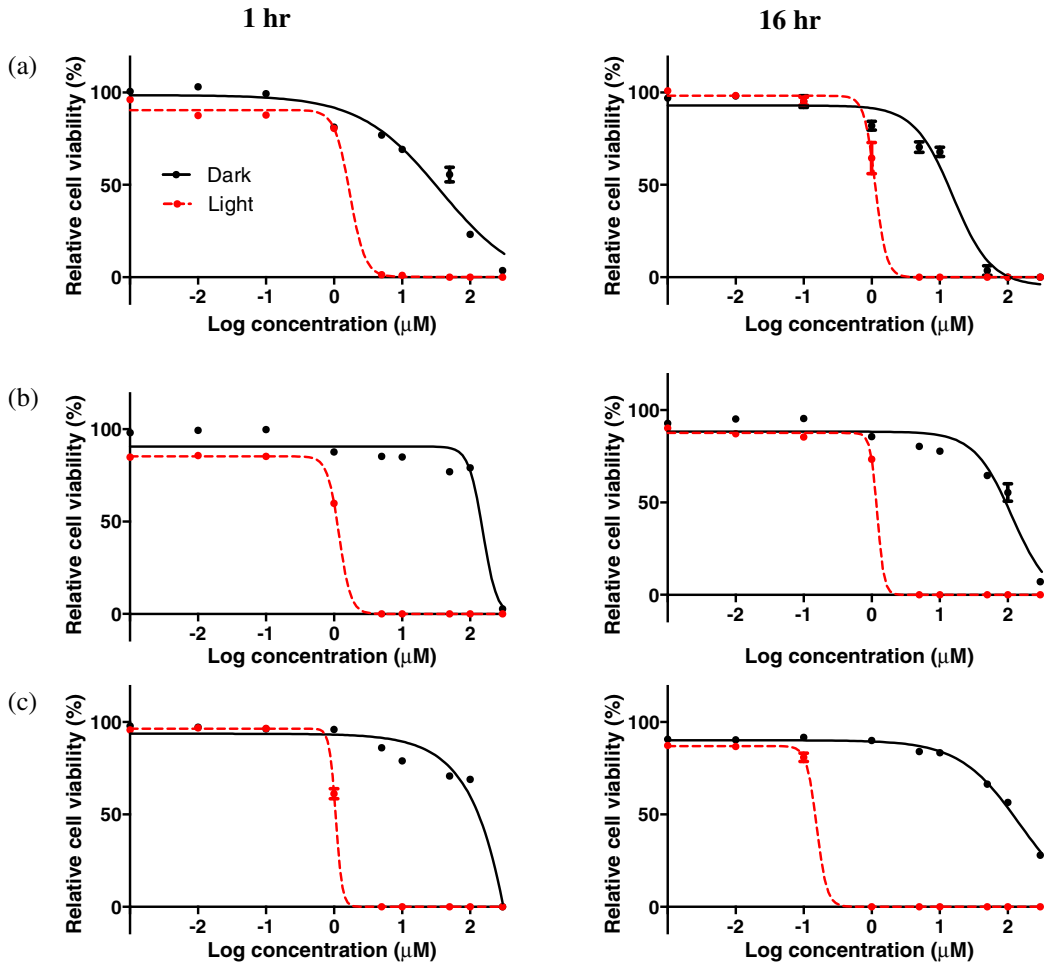


**Fig. 5.** In vitro dose–response curves for compounds **1**–**3** [(a)–(c), respectively] in HL-60 cells with (dashed) and without (solid) a visible light treatment (100 J $cm^{-2}$) and compound-to-light intervals of 1 (left) or 16 h (right).

uptake for the more π-expansive IP–*n*T complexes despite their enhanced lipophilicity. We have observed self-aggregation for α-oligothienyl complexes with $n > 2$, which may slow or impede cellular uptake in the absence of a light trigger.

All three strained metal–organic dyads displayed enhanced cytotoxicity with light exposure. The photocytotoxicity profiles of **1**–**3** were similar ($EC_{50}$ values of 1–2 μM) at short $t_{hν}$ (Table 3, Fig. 5). These differences, however slight, did parallel $^1O_2$ production, with **3** being the most phototoxic at $EC_{50} = 1.1$ μM and the best $^1O_2$ generator. With longer $t_{hν}$ (16 h), the light cytotoxicities for **1** and **2** against HL-60 cells did not change significantly from the shorter interval. However, the potency of **3** increased over five-fold, bringing its activity into the nanomolar regime ($EC_{50} = 200$ nM). Notably, light-activated **3** was over ten-fold more cytotoxic than cisplatin, making it a potent photocisplatin agent with an excellent phototherapeutic margin (PI = 750). The corresponding PIs calculated for **1** and **2** under these conditions were 15 and 96, respectively, which were only slightly attenuated relative to $t_{hν} = 1$ h.

The profound influence of the compound-to-light interval on the photocytotoxicity and PI exhibited by **3** suggests that the longer pre-illumination incubation time may enhance cellular accumulation (and

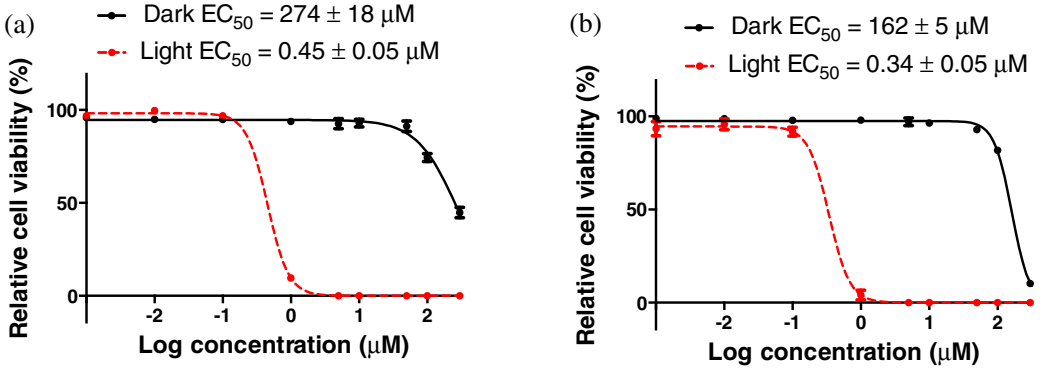


**Fig. 6.** In vitro dose–response curves for melanoma cells (SK-MEL-28) treated with compound **3** in the dark (solid) or exposed to visible light (dashed) of 100 J $cm^{-2}$ with a compound-to-light interval of 1 (left) or 16 h (right).

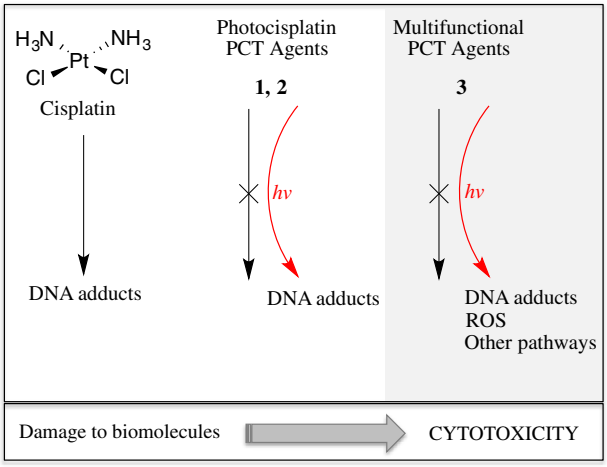


**Scheme 4.** Key results from this study.

membrane interaction), and further supports the notion that its low dark toxicity may arise from reduced cellular uptake in the absence of a light trigger. However, at present we cannot rule out other causal factors (such as localization, relocalization, efflux and/or metabolism) that may be influenced by incubation times.

It is tempting to speculate that the six-fold greater light potency of **3** (relative to **1** and **2**) may be due to its larger capacity for $^1O_2$ production and slower rate of photoejection. When oxygen is available, strained Ru(II) complexes with π-expansive ligands may show a preference for catalytic photosensitization over stoichiometric photoejection, and excited-state energy transfer to form $^1O_2$ may be the most lethal pathway. Moreover, the unstrained congeners of **3** demonstrate the remarkable ability to generate $^1O_2$ even at extremely low oxygen tension due to the very long native lifetimes of their low-energy $^3$IL states [17]. The analogous unstrained counterparts of **1** and **2** do not possess IL states of sufficiently low energy to intercept $^3$MLCT excitons. Therefore, despite a $\Phi_\Delta$ value of more than 30% measured at ambient oxygen levels in a cell-free environment, compound **2** may not maintain this efficiency when cellular oxygen is depleted (PDT is known to induce hypoxia [33]). Consequently, **2** may operate primarily through a photoejection mechanism, and not be capable of the dual action anticipated from a truly multifunctional PCT agent. In this regard, **3** is the only member of the series that shows promise as a dual-action photocisplatin agent. In fact, α-oligothienyl systems of $n > 2$ are known for their redox chemistry and conductive properties (which can be amplified by light), which suggests that more than two mechanisms may contribute to the phototoxic effects elicited by **3**.

Importantly, the photobiological activity of compound **3** extended to other cell lines of interest. Compound **3** elicited a potent PDT effect against melanoma cells (Fig. 6). Upon light activation, compound 3 became a powerful phototoxin, characterized by nanomolar $EC_{50}$ values and PIs as large as 600. This light toxicity could be amplified with longer $t_{hv}$, but the effect was not as pronounced as that observed with HL-60 cells. Similar to the results obtained using leukemia cells, compound **3** was nontoxic to SK-MEL-28 cells without light activation ($EC_{50} > 100$ μM). With longer incubation times, the dark toxicity increased slightly but was still in the range considered nontoxic. These favorable properties have prompted an investigation of strained photocisplatin systems such as **3** as multifunctional PCT agents for melanoma tumors specifically. Melanomas present a challenging microenvironement where dual-action agents, not compromised by oxygen status, are warranted.

## 4. Conclusions

Three strained Ru(II) metal–organic dyads were synthesized and characterized in this study to probe whether such systems are capable of acting as multifunctional light-responsive agents. We found that the 6,6′-dmb ligand provided the steric clash necessary for making dissociative $^3$MC excited states accessible with visible light, and that phototriggered ligand loss was rapid and selective for all three compounds. Photolabilization rates increased with decreasing $n$ on the IP–$n$T ligand in the order **3**<**2**<**1**, and DNA sensitivity toward photoadduct formation with these compounds followed a similar trend. The number of thiophene units on the non-labile IP–$n$T ligand determined $^1O_2$ production, whereby quantum yields increased with $n$, ranging from only 3% for **1** to 42% for **3**. Therefore, π-expansion on the non-labile ligand appears to be an important determinant for dual photobiological action by this class of compounds. Gel mobility shift assays alongside analytical HPLC confirmed that light-activated compound **3** could partition its excited state reactivity between covalent modification of DNA and single-strand breaks. These two complementary modes of DNA damage were attributed to light-triggered ligand loss and sensitization of $^1O_2$, respectively, and translated to selective phototoxicity toward cancer cells. Upon light exposure, all of the compounds were more potent than cisplatin, with **3** exhibiting nanomolar potency with a very large therapeutic margin. We conclude that strained Ru(II) metal–organic dyads with π-expansive ligands derived from α-oligothienyl units of $n > 2$ act as potent photocisplatin agents with through at least two modes of action, and possibly more (Scheme 4). Studies are underway to further explore the scope of strained metal–organic dyads as multifunctional PCT agents.

## Abbreviations

| | |
|---|---|
| C/N | compound-to-nucleotide |
| EC | effective concentration |
| EtBr | ethidium bromide |
| MC | metal-centered |
| PDT | photodynamic therapy |
| PCT | photochemotherapy |
| PACT | photoactivated cancer therapy |
| PS | photosensitizer |
| PI | phototherapeutic index |

## Associated content

Supporting Information. $^1$H and 2D $^1$H–$^1$HCOSY NMR and mass spectra for the Ru(II) complexes, and DNA gel mobility shift assay for cisplatin.

## Acknowledgments

We acknowledge financial support from the Natural Sciences and Engineering Council of Canada, the Canadian Foundation for Innovation, the Nova Scotia Research and Innovation Trust, and Acadia University.

## References

[1] W.R. Wilson, M.P. Hay, Nat. Rev. Cancer 393–410 (2011).
[2] P. Vaupel, A. Mayer, Cancer Metastasis Rev. 26 (2007) 225–239.
[3] R.E. Mahnken, M.A. Billadeau, E.P. Nikonowicz, H.J. Morrison, Am. Chem. Soc. 114 (1992) 9253–9265.
[4] D. Loganathan, H. Morrison, Curr. Opin. Drug Discov. Devel. 8 (2005) 478–486.
[5] E. Wachter, D.K. Heidary, B.S. Howerton, S. Parkin, E.C. Glazer, Chem. Commun. 48 (2012) 9649–9651.
[6] B.S. Howerton, D.K. Heidary, E.C.J. Glazer, Am. Chem. Soc. 134 (2012) 8324–8327.
[7] A.-C. Laemmel, J.-P. Collin, J.-P. Sauvage, Eur. J. Inorg. Chem. (1999) 383–386.
[8] E. Baranoff, J.-P. Collin, J. Furusho, Y. Furusho, A.-C. Laemmel, J.-P. Sauvage, Inorg. Chem. 41 (2012) 1215–1222.
[9] J.D. Knoll, B.A. Albani, C.B. Durr, C.J. Turro, Phys. Chem. A 118 (2014) 10603–10610.
[10] J.D. Knoll, B.A. Albani, C. Turro, Chem. Commun. 51 (2015) 8777–8780.
[11] B.A. Albani, B. Peña, N.A. Leed, N.A.B.G. de Paula, C. Pavani, M.S. Baptista, K.R. Dunbar, C.J. Turro, Am. Chem. Soc. 136 (2014) 17095–17101.
[12] G. Shi, S. Monro, R. Hennigar, J. Colpitts, J. Fong, K. Kasimova, H. Yin, R. DeCoste, C. Spencer, L. Chamberlain, A. Mandel, L. Lilge, S.A. McFarland, Coord. Chem. Rev. 282-283 (2015) 127–138.
[13] H. Yin, M. Stephenson, J. Gibson, E. Sampson, G. Shi, T. Sainuddin, S. Monro, S.A. McFarland, Inorg. Chem. 53 (2014) 4548–4559.

[14] M. Stephenson, C. Reichardt, M. Pinto, M. Wächtler, T. Sainuddin, G. Shi, H. Yin, S. Monro, E. Sampson, B. Dietzek, S.A.J. McFarland, Phys. Chem. A 118 (2014) 10507–10521.
[15] C. Reichardt, M. Pinto, M. Wächtler, M. Stephenson, S. Kupfer, T. Sainuddin, J. Guthmuller, S.A. McFarland, B.J. Dietzek, Phys. Chem. A 119 (2015) 3986–3994.
[16] Y. Arenas, S. Monro, G. Shi, A. Mandel, S. McFarland, L. Lilge, Photodiagn. Photodyn. Ther. 10 (2013) 615–625.
[17] R. Lincoln, L. Kohler, S. Monro, H. Yin, M. Stephenson, R. Zong, A. Chouai, C. Dorsey, R. Hennigar, R.P. Thummel, S.A. McFarland, J. Am. Chem. Soc. 135 (45) (2013) 17161–17175.
[18] S. Monro, J. Scott, A. Chouai, R. Lincoln, R. Zong, R.P. Thummel, S.A. McFarland, Inorg. Chem. 49 (2010) 2889–2900.
[19] J.P. Collin, J.P. Sauvage, Inorg. Chem. 25 (1986) 135–141.
[20] A.N. Hidayatullah, E. Wachter, D.K. Heidary, S. Parkin, E.C. Glazer, Inorg. Chem. 53 (2014) 10030–10032.
[21] E. Wachter, B.S. Howerton, E.C. Hall, S. Parkin, E.C. Glazer, Chem. Commun. 50 (2014) 311–313.
[22] M.C. DeRosa, R.J. Crutchley, Coord. Chem. Rev. 233 (234) (2002) 351–371.
[23] D.T. Croke, L. Perrouault, M.A. Sari, J.-P. Battioni, D. Mansuy, C. Helene, J.J. Le Doan, Photochem. Photobiol. 18 (1993) 41–50.
[24] D. Praseuth, A. Gaudemer, J.-B. Verlhac, I. Kraljic, I. Sissoëff, E. Guillé, Photochem, Photobiol. 44 (1986) 717–724.
[25] L.-F. Tan, F. Wang, H. Chao, Y.-F. Zhou, C. Weng, J. Inorg. Biochem. 101 (2007) 700–708.
[26] P.B. Hitchcock, K.R. Seddon, J.E. Turp, Y.Z. Yousif, J.A. Zora, E.C. Constable, O. Wernberg, J. Chem. Soc. Dalton Trans. 1837–1842 (1988).
[27] B.-H. Ye, X.-M. Chen, T.-X. Zeng, L.-N. Ji, Inorg. Chim. Acta 240 (1995) 5–11.
[28] B. Sun, J. Chu, F. Gao, L.-N. Ji, H. Chao, J. Mol. Struct. 890 (2008) 203–208.
[29] C.-W. Jiang, H. Chao, R.-H. Li, H. Li, L.-N. Ji, Polyhedron 20 (2001) 2187–2193.
[30] J.-Z. Wu, L. Li, T.-X. Zeng, L.-N. Ji, J.-Y. Zhou, T. Luo, R.-H. Li, Polyhedron 16 (1997) 103–107.
[31] M.V. Keck, S.J.J. Lippard, Am. Chem. Soc. 114 (1992) 3386–3390.
[32] M. Demeunynck, C. Bailly, W.D. Wilson, Small Molecule DNA and RNA Binders: From Synthesis to Nucleic Acid Complexes, Wiley-VCH, New York, 2003.
[33] T.H. Foster, R.S. Murant, R.G. Bryant, R.S. Knox, S.L. Gibson, R. Hilf, Radiat. Res. 126 (1991) 296–303.